Astronomy
&
Astrophysics

Massive unseen companions to hot faint underluminous stars from SDSS (MUCHFUSS)

Analysis of seven close subdwarf B binaries[*],[**]

S. Geier[1], P. F. L. Maxted[2], R. Napiwotzki[3], R. H. Østensen[4], U. Heber[1], H. Hirsch[1], T. Kupfer[1], S. Müller[1], A. Tillich[1], B. N. Barlow[5], R. Oreiro[4,6], T. A. Ottosen[7,8], C. Copperwheat[9], B. T. Gänsicke[9], and T. R. Marsh[9]

[1] Dr. Karl Remeis-Observatory & ECAP, Astronomical Institute, Friedrich-Alexander University Erlangen-Nuremberg, Sternwartstr. 7, 96049 Bamberg, Germany
e-mail: geier@sternwarte.uni-erlangen.de
[2] Astrophysics Group, Keele University, Staffordshire, ST5 5BG, UK
[3] Centre of Astrophysics Research, University of Hertfordshire, College Lane, Hatfield AL10 9AB, UK
[4] Institute of Astronomy, K.U. Leuven, Celestijnenlaan 200D, 3001 Heverlee, Belgium
[5] Department of Physics and Astronomy, University of North Carolina, Chapel Hill, NC 27599-3255, USA
[6] Instituto de Astrofísica de Andalucía Glorieta de la Astronomía s/n 18008 Granada, Spain
[7] Department of Physics and Astronomy, Aarhus University, 8000 Aarhus C, Denmark
[8] Nordic Optical Telescope, Apartado 474, 38700 Santa Cruz de La Palma, Santa Cruz de Tenerife, Spain
[9] Department of Physics, University of Warwick, Conventry CV4 7AL, UK

ABSTRACT

The project Massive Unseen Companions to Hot Faint Underluminous Stars from SDSS (MUCHFUSS) aims at finding hot subdwarf stars with massive compact companions like massive white dwarfs ($M > 1.0\,M_{\odot}$), neutron stars or stellar mass black holes. The existence of such systems is predicted by binary evolution theory and recent discoveries indicate that they exist in our Galaxy. First results are presented for seven close binary sdBs with short orbital periods ranging from ≃0.21 d to 1.5 d. The atmospheric parameters of all objects are compatible with core helium-burning stars. The companions are most likely white dwarfs. In one case the companion could be shown to be a white dwarf by the absence of light-curve variations. However, in most cases late type main sequence stars cannot be firmly excluded. Comparing our small sample with the known population of close sdB binaries we show that our target selection method aiming at massive companions is efficient. The minimum companion masses of all binaries in our sample are high compared to the reference sample of known sdB binaries.

Key words. subdwarfs – binaries: spectroscopic – binaries: close – white dwarfs

1. Introduction

Subluminous B stars (sdBs) are core helium-burning stars with very thin hydrogen envelopes and masses around $0.5\,M_{\odot}$ (Heber 1986, see Heber 2009, for a review). A large fraction of the sdB stars (40% to 80%) are members of short period binaries (Maxted et al. 2001; Napiwotzki et al. 2004a). Several studies were undertaken to determine the orbital parameters of subdwarf binaries, and found periods ranging from 0.07 to more than 10 d with a peak at 0.5 to 1.0 d (e.g. Edelmann et al. 2005; Morales-Rueda et al. 2003). For close binary sdBs, common envelope (CE) ejection is the most probable formation channel. In this scenario two main sequence stars of different masses evolve in a binary system. The heavier one will reach the red giant phase first and fill its Roche lobe. If the mass transfer to the companion is dynamically unstable, a common envelope is formed. Due to friction the two stellar cores lose orbital energy, which is deposited within the envelope and leads to a shortening of the binary period. Eventually the common envelope is ejected and a close binary system is formed, which contains a core helium-burning sdB and a main sequence companion. If the companion has already evolved to a white dwarf (WD) when the red giant fills its Roche lobe, a close sdB+WD binary is formed (Han et al. 2002, 2003). Under certain conditions, two consecutive CE phases are possible as well.

In general it is difficult to put constraints on the nature of the close companions to sdB stars. Since most of the binaries are single-lined, only lower limits have been derived from the binary mass functions, which are in general compatible with main sequence stars of spectral type M or compact objects like white dwarfs. Only in special and hence rare cases can tighter constraints be put on the nature of the companions.

Subdwarf binaries with massive WD companions turned out to be candidates for supernova type Ia (SN Ia) progenitors because these systems lose angular momentum due to the emission of gravitational waves and start mass transfer. This mass transfer, either from accretion of He onto the WD during the sdB phase (e.g. Yoon & Langer 2004, and references therein), or the subsequent merger of the system after the sdB star itself has turned into a WD (Tutukov & Yungelson 1981; Webbink 1984) may cause the companion to approach the Chandrasekhar limit and explode as SN Ia.

SN Ia play a key role in the study of cosmic evolution (e.g. Riess et al. 1998; Leibundgut 2001; Perlmutter et al. 1999). One of the best known candidate systems for the double degenerate merger scenario is the sdB+WD binary KPD 1930+2752 (Maxted et al. 2000a; Geier et al. 2007). Mereghetti et al. (2009) showed that in the X-ray binary HD 49798 a massive ($>1.2\,M_\odot$) white dwarf accretes matter from a closely orbiting subdwarf O companion. The predicted amount of accreted material is sufficient for the WD to reach the Chandrasekhar limit. This makes HD 49798 another candidate for SN Ia progenitor. Furthermore, Perets et al. (2010) showed that helium accretion onto a white dwarf may be responsible for a subclass of faint and calcium-rich SN Ib events.

Geier et al. (2008, 2010a,b) analysed high resolution spectra of sdB stars in close binaries. Assuming synchronised rotation they constrained the masses and the nature of the unseen companions in 31 cases. While most of the derived companion masses were consistent with either late type main sequence stars or white dwarfs, the compact companions of some sdBs may be either massive white dwarfs, neutron stars (NS) or stellar mass black holes (BH). However, Geier et al. (2010b) also showed that the assumption of orbital synchronisation in close sdB binaries is not always justified and that their analysis suffers from huge selection effects.

The existence of sdB+NS/BH systems is predicted by binary evolution theory (Podsiadlowski et al. 2002; Pfahl et al. 2003). The formation channel includes two phases of unstable mass transfer and one supernova explosion. The fraction of sdB+NS/BH systems is predicted to be about 2% of the close sdB binaries (Geier et al. 2010b). Yungelson & Tutukov (2005) and Nelemans (2010) performed independent binary evolution calculations and confirm that sdB+NS/BH systems should exist. According to the results of Nelemans (2010) about 1% of the subdwarfs in close binaries should have a neutron star companion, whereas only 0.01% should be orbited by a black hole. Yungelson & Tutukov (2005) predict the sdB+NS fraction to be of the order of 0.8%.

Since sdB stars eventually evolve to WDs there should also exist a population of white dwarfs with massive compact companions. Badenes et al. (2009) reported the discovery of a close binary consisting of a massive white dwarf and an unseen neutron star or black hole companion, but Marsh et al. (2010) most recently showed that the system is double-lined and consists of a massive white dwarf orbited by a low mass white dwarf. The system mass is below the Chandrasekhar limit. Their results were confirmed by Kulkarni & van Kerkwijk (2010). Common envelope ejection was proposed as the most likely formation channel

Table 1. Solved binary systems.

SDSS name	Short name	Other names
SDSS J002323.99−002953.2	J0023−0029	PB 5916
SDSS J113840.68−003531.7	J1138−0035	PG 1136-003
SDSS J150513.52+110836.6	J1505+1108	PG 1502+113
SDSS J165404.25+303701.7	J1654+3037	PG 1652+307
SDSS J172624.09+274419.3	J1726+2744	PG 1724+278
SDSS J204613.40−045418.7	J2046−0454	–
SDSS J225638.34+065651.0	J2256+0656	PG 2254+067

for the binary PSR J1802−2124, which consists of a millisecond pulsar and a CO white dwarf in close orbit ($P = 0.7$ d, Ferdman et al. 2010). This peculiar system may have evolved through an earlier sdB+NS phase.

2. The MUCHFUSS project

The discovery of sdB binary candidates with massive compact companions provides a first hint that a whole population of non-interacting binaries with such companions may be present in our Galaxy. The known candidate sdB+NS/BH binaries have low orbital inclinations (15−30°, Geier et al. 2010b). High inclination systems must exist as well and should be more numerous. In this case a determination of the orbital parameters is sufficient to put a lower limit to the companion mass by calculating the binary mass function. If this lower limit exceeds the Chandrasekhar mass and no sign of a companion is visible in the spectra, the existence of a massive compact companion is proven without the need for any additional assumptions.

The project Massive Unseen Companions to Hot Faint Underluminous Stars from SDSS[1] (MUCHFUSS) aims at finding sdBs with compact companions like massive white dwarfs ($M > 1.0\,M_\odot$), neutron stars or black holes. About 70 binaries have been selected for follow-up. Survey and target selection are described in detail in Geier et al. (2010c). The same selection criteria that we applied to find such binaries are also well suited to single out hot subdwarf stars with constant high radial velocities (RV) in the Galactic halo and search for hypervelocity stars. First results of this second part of the project (Hyper-MUCHFUSS) are presented in Tillich et al. (2010).

Here we present the spectroscopic analysis of the first sdB binaries discovered in the course of the MUCHFUSS project (see Table 1). In Sect. 3 the observations and the data reduction are described. Sections 4 and 5 deal with the determination of the orbital and atmospheric parameters of the sdB stars. Section 6 explains the way the minimum masses of the unseen companions are constrained, while results are presented in Sect. 7. The efficiency of our target selection is discussed in Sect. 8, a short summary and an outlook are eventually given in Sect. 9.

3. Multi-site observations and data reduction

Follow-up medium resolution spectra were taken during dedicated follow-up runs (see Table 2) with the EFOSC2 spectrograph ($R \simeq 2200$, $\lambda = 4450−5110$ Å) mounted at the ESO NTT,

---

[1] Sloan Digital Sky Survey.
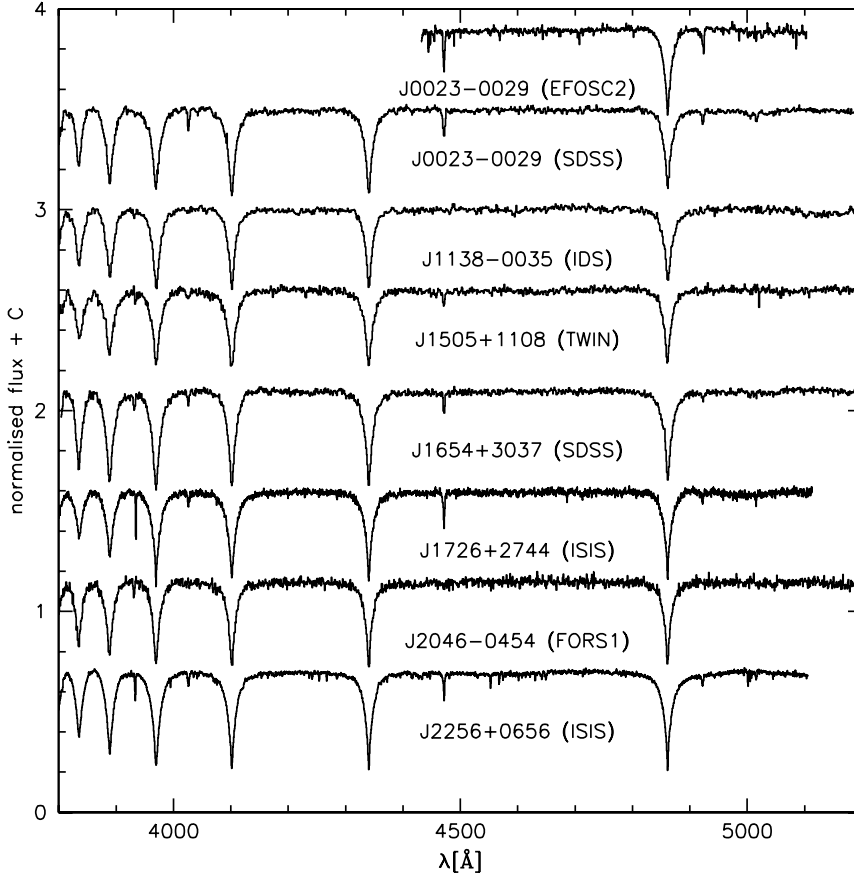
Fig. 1. Medium resolution spectra of the programme stars taken with different instruments. Multiple observations of the same target have been shifted to rest wavelength and coadded.

Table 2. Follow-up observations 2009/2010.

Date	Telescope & Instrument	Observer
2009/06/05–2009/06/09	ING-INT/IDS	R. Ø., R. O., T. O.
2009/07/22–2009/07/26	CAHA-3.5m/TWIN	T. K.
2009/08/24–2009/08/27	ING-WHT/ISIS	S. G.
2009/11/08–2009/11/12	ESO-NTT/EFOSC2	T. K.
April/August 2009	Gemini-North/GMOS	Service
2010/02/12–2010/02/15	SOAR/Goodman	B. B.

Notes. The first column lists the date of observation, while in the second the used telescope and instrumentation is shown. In the third column the observers are listed.

the ISIS spectrograph ($R \simeq 4000, \lambda = 3440-5270$ Å) mounted at the WHT, the TWIN spectrograph mounted at the CAHA-3.5 m telescope ($R \simeq 4000, \lambda = 3460-5630$ Å), the Goodman spectrograph mounted at the SOAR telescope ($R \simeq 2500, \lambda = 3500-6160$ Å), the GMOS spectrograph ($R \simeq 1200, \lambda = 3770-4240$ Å) mounted at the Gemini North telescope and the IDS spectrograph mounted at the Isaac Newton Telescope ($R \simeq 1400, \lambda = 3000-6800$ Å). Informations about data taken in the course of our survey are provided in Geier et al. (2010c). Additional data could be gathered, when our targets were observed with the IDS spectrograph (March 2007, observer: T. M., C. C.; $R \simeq 4000, \lambda = 3930-5100$ Å) and the grating spectrograph (March 2003, April 2004, observer: T. M.; $R \simeq 4600, \lambda = 4170-5030$ Å) mounted at the 1.9 m Radcliffe Telescope. Example spectra are shown in Fig. 1.

In order to obtain a good wavelength calibration, arc lamp exposures have been taken before or after the single exposures.

In addition to that bright single sdBs have been taken as RV standards in most of the runs. In some cases the RVs of certain instruments (TWIN, GMOS) had to be corrected by a constant offset of up to $\simeq 50$ km s^{-1}, which was derived from the RV measurements of the standard stars. The slit width was always chosen to be smaller than the size of the seeing discs to minimize systematic errors due to movement of the objects within the slit. Reduction was done either with the `MIDAS`, `IRAF` or `PAMELA`[2] and `MOLLY`[2] packages.

4. Orbital parameters

The radial velocities were measured by fitting a set of mathematical functions (Gaussians, Lorentzians and polynomials) to the hydrogen Balmer lines as well as helium lines if present using the FITSB2 routine (Napiwotzki et al. 2004b). The RVs of the GMOS spectra have been measured by fitting three Gaussians to the H_γ line. Three functions are used to match the continuum, the line and the line core, respectively and mimic the typical Voigt profile of spectral lines. The profiles are fitted to all suitable lines simultaneously using χ^2-minimization and the RV shift with respect to the rest wavelengths is measured. The RVs and formal 1σ-errors are given in Appendix B. Assuming circular orbits sine curves were fitted to the RV data points in fine steps over a range of test periods. For each period the χ^2 of the best fitting sine curve was determined. The result is similar to a power spectrum with the lowest χ^2 indicating the most likely period (see Fig. 4). In order to estimate the significance of the orbital solutions and the contributions of systematic effects to the

---

[2] http://www2.warwick.ac.uk/fac/sci/physics/research/astro/people/marsh/software

Table 3. Derived orbital parameters.

Object	T_0 [−2 450 000]	P [d]	γ [km s^{-1}]	K [km s^{-1}]
J0023−0029	5069.850 ± 0.008	1.4876 ± 0.0001	16.4 ± 2.1	81.8 ± 2.9
J1138−0035	4991.388 ± 0.001	0.207536 ± 0.000002	23.3 ± 3.7	162.0 ± 3.8
J1505+1108	4938.867 ± 0.002	0.74773 ± 0.00005	−77.1 ± 1.2	97.2 ± 1.8
J1654+3037	4991.5322 ± 0.0008	0.25357 ± 0.00001	40.5 ± 2.2	126.1 ± 2.6
J1726+2744	4981.667 ± 0.005	0.50198 ± 0.00005	−36.7 ± 4.8	118.9 ± 3.7
J2046−0454	4693.352 ± 0.002	0.24311 ± 0.00001	87.6 ± 5.7	134.3 ± 7.8
J2256+0656	5070.662 ± 0.002	0.7004 ± 0.0001	−7.3 ± 2.1	105.3 ± 3.4

Table 4. Significance of the circular orbital solutions.

Object	Best solution [d]	χ^2	χ^2_{reduced}	2nd best alias [d]	$\Delta\chi^2$	n	e_{norm} [km s^{-1}]	$\log p_{\text{false}}[1\%]$	$\log p_{\text{false}}[10\%]$
J0023−0029	1.4876	157	3.74	0.5976	130	47	8.0	−3.0	−3.4
J1138−0035	0.207536	213	5.33	0.260192	426	45	16.0	−3.5	−3.5
J1505+1108	0.74773	155	4.30	0.75709	679	41	7.0	<−4.0	<−4.0
J1654+3037	0.25357	18	0.54	0.20397	64	38	−	<−4.0	
J1726+2744	0.50198	82	2.48	1.00998	77	38	12.0	−1.2	−1.9
J2046−0454	0.24311	52	3.05	0.31971	39	22	17.0	−1.1	−1.1
J2256+0656	0.7004	276	6.13	2.1903	976	50	13.0	<−4.0	<−4.0

Notes. The best solutions for the orbital periods are given together with their minimum χ^2 and reduced χ^2 values as well as the number n of RVs. The second best aliases (further than 1% away from the best solution) and the $\Delta\chi^2$-values with respect to the best solutions are given as well. The systematic error adopted to normalise the reduced χ^2 (e_{norm}) is given for each case. The probabilities for the orbital period to deviate from our best solution by more than 1% ($p_{\text{false}}[1\%]$) or 10% ($p_{\text{false}}[10\%]$) are given in the last columns.

error budget, we normalised the χ^2 of the most probable solution by adding systematic errors in quadrature until the reduced χ^2 reached ≃1.0. Using these modified uncertainties we performed Monte Carlo simulations for the most likely periods. For each simulation a randomised set of RVs was drawn from Gaussian distributions with central value and width corresponding to the RV measurements and the analysis repeated. From these simulations the probabilities for the orbital periods to deviate from our best solution by more than 1% or 10% were calculated.

In order to derive most conservative errors for the RV semi-amplitude K and the system velocity γ we fixed the most likely period and created new RV datasets with a bootstrapping algorithm. Ten thousand RV datasets were obtained by random sampling with replacement from the original dataset. In each case an orbital solution was calculated in the way described above. The standard deviation of these results was adopted as error estimate. The RV curves are given in Figs. 2 and 3. The residuals of the RV curves after subtracting the best orbital solution are of the same order in all cases (see Figs. 2, 3). The accuracy is limited by the resolution of the spectra and their signal-to-noise. Combining data obtained with different instruments is also expected to contribute to the systematic error. Nevertheless, we found that all orbital solutions given here are significant (see Tables 3, 4).

Edelmann et al. (2005) reported the discovery of small eccentricities ($e < 0.06$) in the orbital solutions of five close hot subdwarf binaries. All of these binaries are expected to have formed via common envelope ejection. Although the CE phase is very short, it should nevertheless be very efficient in circularising the binary orbits. That is why the discovery of Edelmann et al. (2005) came as a surprise. Napiwotzki et al. (in prep.) found more such systems with even shorter periods.

In order to investigate whether the orbital solutions of our programme binaries can be improved by allowing for eccentricity, we fitted eccentric orbits to our radial velocity data and performed statistical tests (F-test, see Pringle 1975, and the Bayesian information criterion BIC) to check whether eccentric solutions are significant or not. In all cases the circular solutions were preferred. However, the derived upper limits for the orbital eccentricities range from 0.15 to 0.3, which means that low eccentricities as the ones reported by Edelmann et al. (2005) cannot be firmly excluded.

5. Atmospheric parameters

Atmospheric parameters have been determined by fitting model spectra to the hydrogen Balmer and helium lines in the way described in Geier et al. (2007). The single spectra have been corrected for their orbital motion and coadded. Depending on the effective temperature of the stars, LTE models with solar metallicity ($T_{\text{eff}} < 30\,000$ K) or ten times solar metallicity ($T_{\text{eff}} > 30\,000$ K) have been used. The enhanced metallicity models account for the radiative levitation of heavy elements in the diffusion dominated atmospheres (for a detailed discussion see O'Toole & Heber 2006).

In order to investigate systematic effects introduced by the individual instruments, especially the different resolutions and wavelength coverages, the parameters have been derived separately from spectra taken with different instruments. As can be seen in Table A.1 no constant systematic shifts are present. The weighted means have been calculated and adopted as final solutions. Typical systematic errors introduced by different model grids are of the order of ±0.05 in $\log g$ and 500 K in T_{eff} (e.g. Lisker et al. 2005; Geier et al. 2007). These uncertainties were added in quadrature to the statistical errors.

Three of our programme stars have been classified as hot subdwarfs by Eisenstein et al. (2006), but the authors pointed out that the atmospheric parameters of the sdO/Bs given in their catalogue are not accurate.

All stars of our sample are situated on or near the Extreme Horizontal Branch (EHB) and are most likely core-helium burning stars (see Fig. 5). Since the orbital periods of these binaries
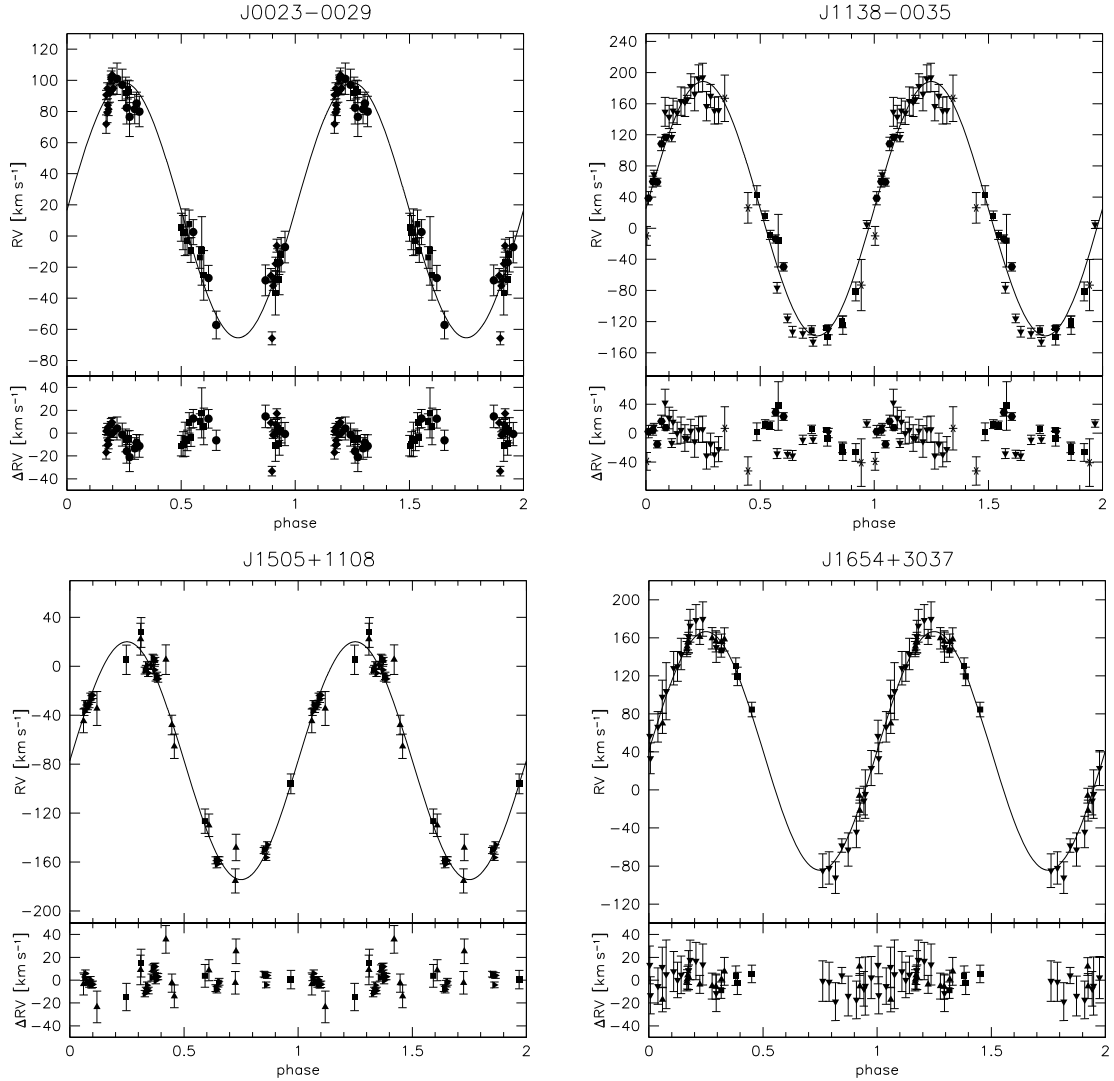
Fig. 2. Radial velocity plotted against orbital phase. The RV data were phase folded with the most likely orbital periods. The residuals are plotted below. The RVs were measured from spectra obtained with SDSS (rectangles), CAHA3.5 m/TWIN (upward triangles), WHT/ISIS (diamonds), INT/IDS (downward triangles), ESO-VLT/FORS1 (triangles turned to the left), Gemini/GMOS (triangles turned to the right), ESO-NTT/EFOSC2 (circles), SOAR/Goodman (hexagons) and SAAO-1.9 m/Grating (stars).

are short, they can only have formed via common envelope ejection. Population synthesis models (Han et al. 2002, 2003) predict a mass range of $M_{sdB} = 0.37–0.48\,M_\odot$ for sdBs in binaries formed in this way. The mass distribution shows a sharp peak at a mass of about $0.47\,M_\odot$. This theoretical mass distribution is consistent with analyses of close binary systems (e.g. Geier et al. 2007; For et al. 2010) as well as asteroseismic analyses of pulsating sdBs (see Charpinet et al. 2008, and references therein). If the progenitor star was massive enough on the main sequence to ignite core helium-burning under non-degenerate conditions, the sdB mass may be as low as $0.3\,M_\odot$. A small fraction of the sdB population is predicted to be formed in that way (Han et al. 2002, 2003). Especially for sdB binaries with massive companions this formation scenario may become important.

## 6. Constraining the nature of the unseen companions

Since the programme stars are single-lined spectroscopic binaries, only their mass functions can be calculated.

$$f_{m} = \frac{M_{comp}^3 \sin^3 i}{(M_{comp} + M_{sdB})^2} = \frac{PK^3}{2\pi G} \,. \qquad (1)$$

Although the RV semi-amplitude K and the period P can be derived from the RV curve, the sdB mass M_{sdB}, the companion mass M_{comp} and the inclination angle i remain free parameters. Adopting $M_{sdB} = 0.47\,M_\odot$ and $i < 90°$ we derive a lower limit for the companion mass (see Table 5).
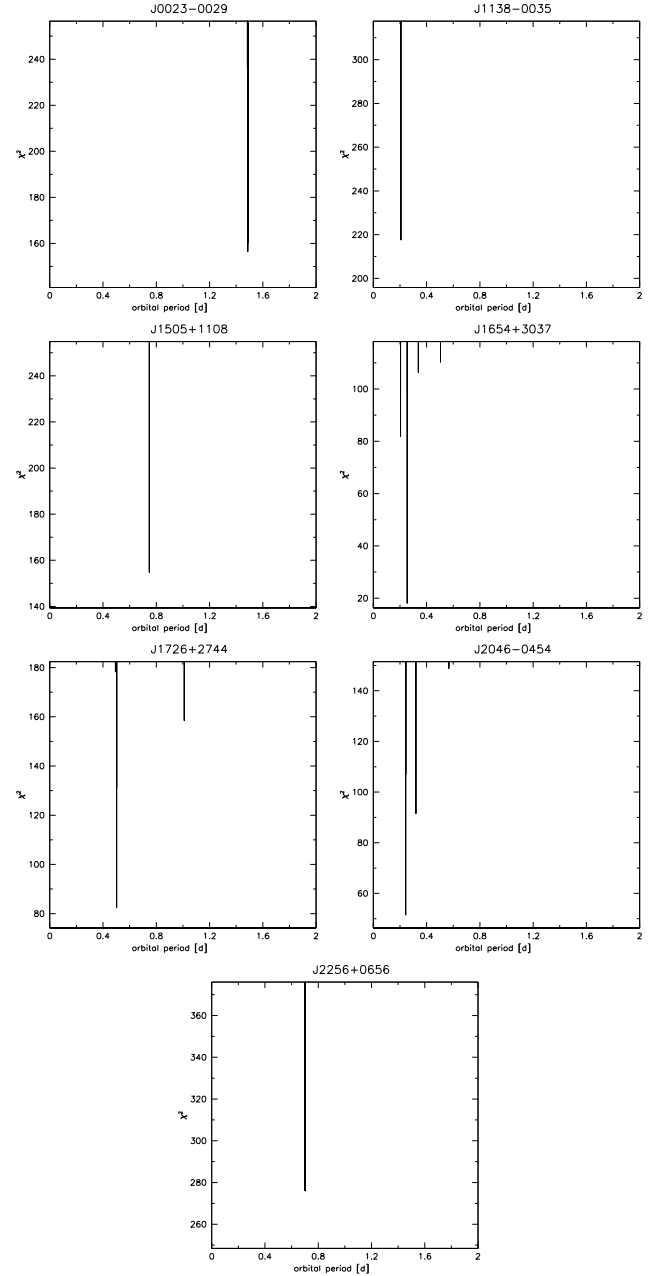
For minimum companion masses lower than $0.45\,M_\odot$ the companion may be a late type main sequence star or a compact object like a WD. Main sequence stars in this mass range are outshined by the sdBs and not visible in optical spectra (Lisker et al. 2005). That is the reason why the companions' nature still remains unknown for most of the $\simeq 80$ known sdB systems with low minimum companion masses (see Fig. 7). If on the other hand the minimum companion mass exceeds $0.45\,M_\odot$, spectral features of a main sequence companion become visible in the optical. The non-detection of such features therefore allows us to exclude a main sequence star. The companion must then be a compact object. More massive compact companions like massive WDs, neutron stars or black holes are more likely as soon as the minimum mass exceeds $1.00\,M_\odot$ or even the Chandrasekhar limit $1.40\,M_\odot$.

Due to the fact that we selected targets with high RV shifts, the distribution of orbital inclinations in our target sample is
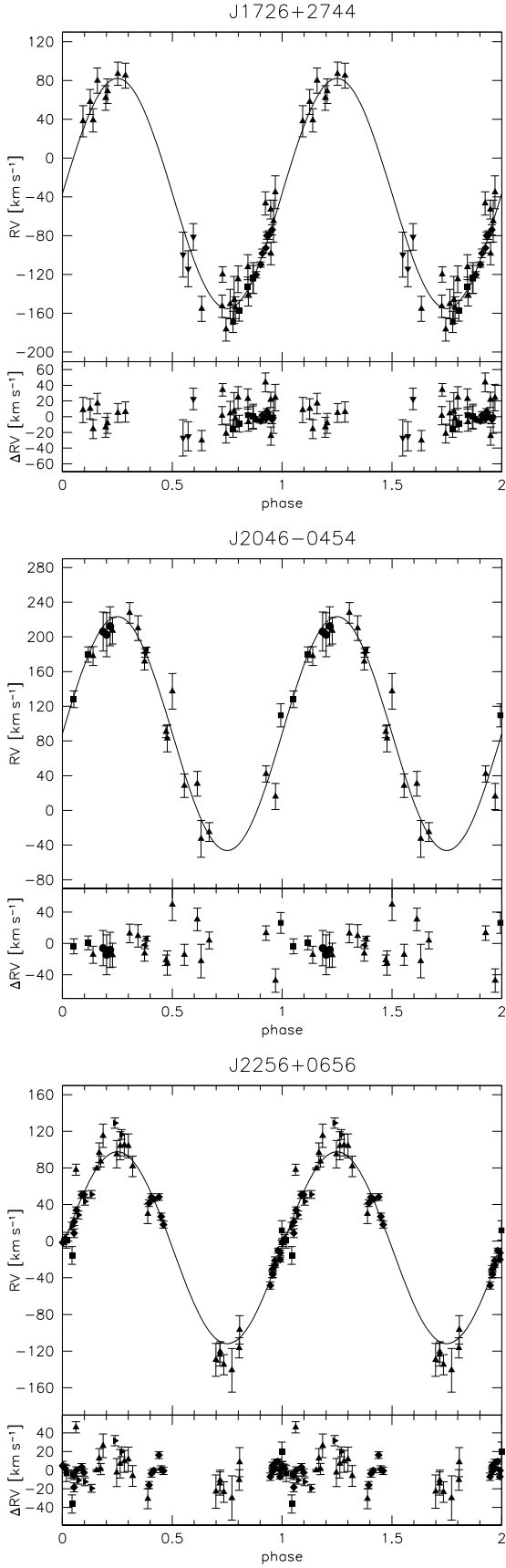
Fig. 3. Radial velocity curves (see Fig. 2).

Fig. 4. χ^2 plotted against orbital period. The lowest peak corresponds to the most likely solution.

Table 5. Derived minimum masses and most probable nature of the companions.

Object	$f(M)$ $[M_\odot]$	$M_{2\mathrm{min}}$ $[M_\odot]$	Companion
J0023−0029	0.084	0.40	MS/WD
J1138−0035	0.091	0.42	WD
J1505+1108	0.071	0.37	MS/WD
J1654+3037	0.053	0.32	MS/WD
J1726+2744	0.087	0.41	MS/WD
J2046−0454	0.061	0.34	MS/WD
J2256+0656	0.085	0.40	MS/WD

not random any more. Our selection strategy strongly favours high inclination angles, and therefore the companion masses are likely to be close to their 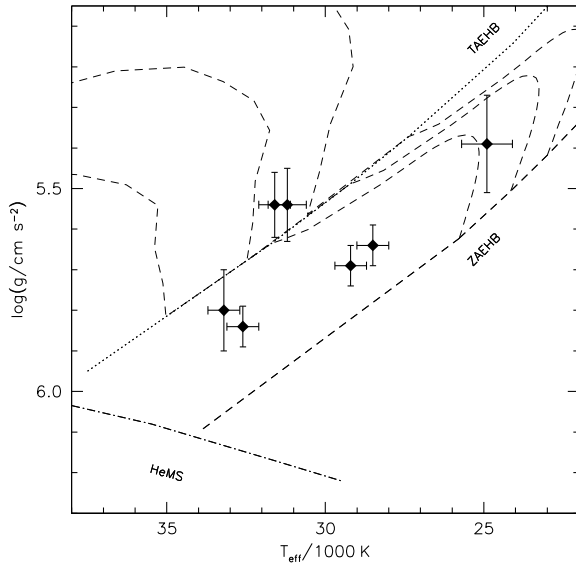minimum values. The probability of detecting eclipses, reflection effects or variations caused by ellipsoidal deformation in the light curves of systems with short orbital periods should therefore be significantly higher than in an unbiased sample.

Fig. 5. $T_{\rm eff} - \log g$-diagram. The helium main sequence (HeMS) and the EHB band (limited by the zero-age EHB, ZAEHB, and the terminal-age EHB, TAEHB) are superimposed with EHB evolutionary tracks from Dorman et al. (1993).
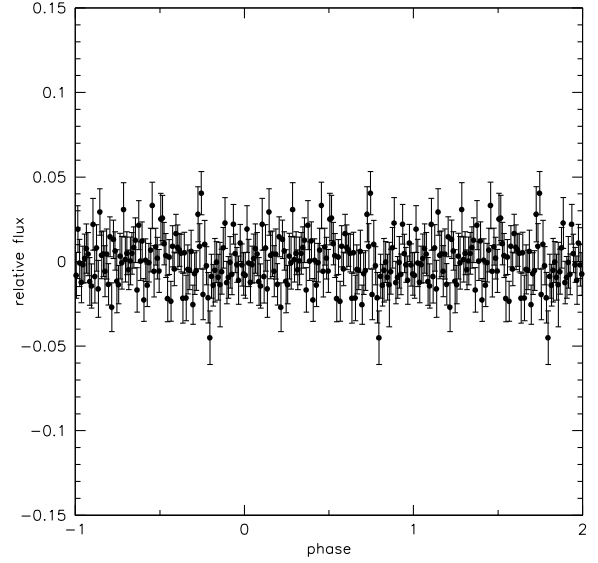
Fig. 6. SuperWASP light curve of J1138−0035 folded to the orbital phase. The 11213 data points taken between 2006/07/05 and 2009/07/02 are binned to 100 phase bins. Relative flux is plotted against the orbital phase.

7. Results

The spectra of all stars in our sample have been checked for spectral features of their companions. Hot subdwarfs with faint main sequence companions usually show spectral lines of the Mg I triplet at ≃5170 Å (Lisker et al. 2005) and the Ca II triplet at ≃8650 Å. No such features are visible in the spectra of our programme stars (see e.g. Fig. 1). Stark & Wade (2003) analysed optical and IR photometry (2MASS) and found no indication of an IR-excess caused by a cool companion in the case of J1654+3037. According to the catalogue of Reed & Stiening (2004), who performed a similar analysis, J1505+1108 shows signs of an IR-excess in the H and K-bands, but the large errors of these measurements and the missing spectral signatures of a cool companion in the SDSS spectra are strong indications, that no visible companion is present.

J1654+3037 and J2046−0454 have very similar orbital parameters. The periods are short (0.25 d) and the minimum companion masses are constrained to 0.32 $M_\odot$ and 0.34 $M_\odot$. Whether the companions are M dwarfs or WDs is therefore not yet clear. In the former case a reflection effect should be easily detectable in the light curves. Photometric follow-up will allow us to clarify the nature of the companions.

The companion of the short period (0.2 d) system J1138−0035 is most likely a white dwarf. The minimum companion mass is constrained to 0.42 $M_\odot$ and no sign of a companion is seen in the spectra. A light curve taken by the SuperWASP project (Pollacco et al. 2006) shows no variation exceeding ≃1% (see Fig. 6). Due to the short period of this system a reflection effect should be visible, if the companion should be a cool main sequence star. The absence of such a variation leads to the conclusion that the companion is most likely a white dwarf.

The orbital periods of J1726+2744 (0.5 d), J2256+0656 (0.7 d) and J1505+1108 (0.75 d) are longer. Their minimum companion masses are similar (0.37−0.41 $M_\odot$) and close to the border between main sequence stars and white dwarfs. The companions of J1726+2744 and J2256+0656 are most likely WDs. Koen (2009) and Shimanskii et al. (2008) recently showed that

reflection effects can still be detected in the light curves of sdB binaries with similar orbital periods. A reflection effect in J0023−0029 on the other hand is most likely not detectable, because the orbital period is too long (1.5 d).

8. Efficiency of target selection

The goal of the MUCHFUSS project is to find sdB binaries with massive compact companions and study this population of close binaries. We tried to optimise our target selection to achieve this goal. Figure 7 illustrates the efficiency of our target selection. The RV semiamplitudes of all known sdB binaries with spectroscopic solutions (open symbols) are plotted against their orbital periods (Geier et al. 2010c). Binaries which have initially been discovered in photometric surveys due to indicative features in their light curves (eclipses, reflection effects, ellipsoidal variations) are marked with open circles. Binaries discovered by RV variations from time resolved spectroscopy are marked with open diamonds. The dashed, dotted and solid lines mark the regions to the right where the minimum companion masses derived from the binary mass function (assuming 0.47 $M_\odot$ for the sdBs) exceed 0.45 $M_\odot$, 1.00 $M_\odot$ and 1.40 $M_\odot$.

Most of the known sdB binaries are situated beneath the 0.45 $M_\odot$ line, which means that the companion type cannot be constrained from the mass function alone. Photometry is necessary to clarify the companions' nature in these cases. The most massive sdB binary known to date is KPD 1930+2752 with a WD companion of 0.9 $M_\odot$. This short period system has been discovered based on indicative features in its light curve (upper left corner in Fig. 7; Billères et al. 2000).

The seven binaries from the MUCHFUSS project are marked with filled diamonds. It can be clearly seen that they belong to the sdB binary population with the largest minimum masses close to 0.45 $M_\odot$. We therefore conclude that our target selection is efficient and singles out sdB binaries with massive companions.
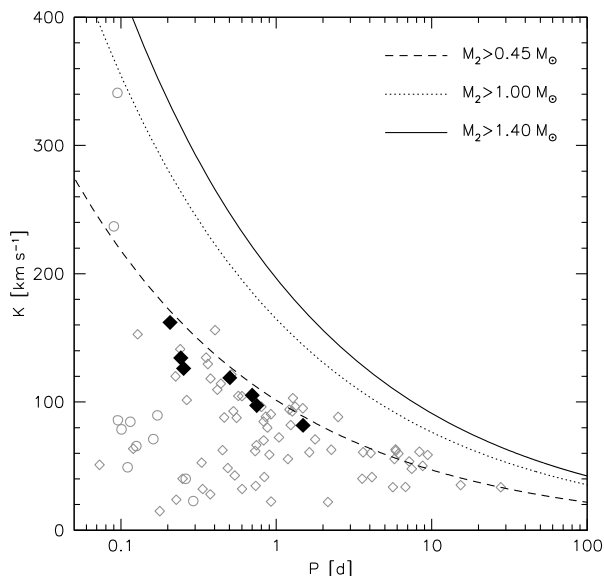
Fig. 7. The RV semiamplitudes of all known sdB binaries with spectroscopic solutions plotted against their orbital periods (Geier et al. 2010c). Binaries which have initially been discovered in photometric surveys due to indicative features in their light curves (eclipses, reflection effects, ellipsoidal variations) are marked with open circles. Binaries discovered by detection of RV variations from time resolved spectroscopy are marked with open diamonds. The dashed, dotted and solid lines mark the regions to the right where the minimum companion masses derived from the binary mass function (assuming $0.47\,M_\odot$ for the sdBs) exceed $0.45\,M_\odot$, $1.00\,M_\odot$ and $1.40\,M_\odot$. The seven binaries from the MUCHFUSS project are marked with filled diamonds.

9. Summary and outlook

A multi-site follow-up campaign is being conducted with medium resolution spectrographs mounted at several different telescopes of mostly 2 m to 4 m-class. First results were presented for seven close binary sdBs with short orbital periods ranging from $\simeq 0.21$ d to 1.5 d and most likely compact companions. The atmospheric parameters of all objects are compatible with core helium-burning stars on the EHB. Comparing our small sample with the known population of close sdB binaries we are able to show that our target selection method is efficient. All binaries solved up to now have high minimum companion masses compared to the rest of the sdB binary population.

Up to now we have found significant orbital solutions for about 10% of our target sample. Photometric follow-up observations will allow us to clarify the nature of the companions in most cases. A database of more than 700 spectra has been built up and some binaries will be solvable with only a few additional RV points.

References

Badenes, C., Mullally, F., Thompson, S. E., & Lupton, R. H. 2009, ApJ, 707, 971
Billères, M., Fontaine, G., Brassard, P., et al. 2000, ApJ, 530, 441
Charpinet, S., van Grootel, V., Reese, D., et al. 2008, A&A, 489, 377
Dorman, B., Rood, R. T., & O'Connell, R. W. 1993, ApJ, 419, 596
Edelmann, H., Heber, U., Altmann, M., Karl, C., & Lisker, T. 2005a, A&A, 442, 1023
Eisenstein, D. J., Liebert, J. L., Harris, H. C., et al. 2006, ApJS, 167, 40
Ferdman, R. D., Stairs, I. H., Kramer, M., et al. 2010, ApJ, 711, 764
For, B.-Q., Green, E. M., Fontaine, G., et al. 2010, ApJ, 708, 253
Geier, S., Heber, U., Kupfer, T., & Napiwotzki, R. 2010a, A&A, 515, A37
Geier, S., Heber, U., Podsiadlowski, Ph., et al. 2010b, A&A, 519, A25
Geier, S., Hirsch, H., Tillich, A., et al. 2010c, A&A, submitted
Geier, S., Nesslinger, S., Heber, U., et al. 2007, A&A, 464, 299
Geier, S., Nesslinger, S., Heber, U., et al. 2008, A&A, 477, L13
Han, Z., Podsiadlowski, P., Maxted, P. F. L., Marsh, T. R., & Ivanova, N. 2002, MNRAS, 336, 449
Han, Z., Podsiadlowski, P., Maxted, P. F. L., & Marsh, T. R. 2003, MNRAS, 341, 669
Heber, U. 1986, A&A, 155, 33
Heber, U. 2009, ARA&A, 47, 211
Koen, C. 2009, MNRAS, 393, 1370
Kulkarni, S. R., & van Kerkwijk, M. H. 2010, ApJ, 719, 1123
Leibundgut, B. 2001, ARA&A, 39, 67
Lisker, T., Heber, U., Napiwotzki, R., et al. 2005, A&A, 430, 223
Marsh, T. R., Gaensicke, B. T., Steeghs, D., et al. 2010, ApJL, submitted [arXiv:1002.4677]
Maxted, P. F. L., Marsh, T. R., & North, R. C. 2000, MNRAS, 317, L41
Maxted, P. F. L., Heber, U., Marsh, T. R., & North, R. C. 2001, MNRAS, 326, 139
Mereghetti, S., Tiengo, A., Esposito, P., et al. 2009, Science, 325, 1222
Morales-Rueda, L., Maxted, P. F. L., Marsh, T. R., North, R. C., & Heber, U. 2003, MNRAS, 338, 752
Napiwotzki, R., Karl, C., Lisker, T., et al. 2004a, Ap&SS, 291, 321
Napiwotzki, R., Yungelson, L., Nelemans, G., et al. 2004b, ASP Conf. Ser., 318, 402
Nelemans, G. 2010, Ap&SS, 329, 25
O'Toole, S. J., & Heber, U. 2006, A&A, 452, 579
Perets, H. B., Gal-Yam, A., Mazzali, P. A., et al. 2010, Nature, 465, 322
Perlmutter, S., Aldering, G., Goldhaber, G., et al. 1999, ApJ, 517, 565
Pfahl, E., Rappaport, S., & Podsiadlowski, Ph. 2003, ApJ, 597, 1036
Podsiadlowski, Ph., Rappaport, S., & Pfahl, E. D. 2002, ApJ, 565, 1107
Pollacco, D. L., Skillen, I., Cameron, A. C., et al. 2006, PASP, 118, 1407
Pringle, J. E. 1975, MNRAS, 170, 633
Reed, M. D., & Stiening, R. 2004, PASP, 116, 506
Riess, A. G., Fillipenko, A. V., Challis, P., et al. 1998, AJ, 116, 1009
Shimanskii, V. V., Bikmaev, I. F., Borisov, N. V., et al. 2008, ARep, 52, 729
Stark, M. A., & Wade, R. A. 2003, AJ, 126, 1455
Tillich, A., Heber, U., Geier, S., et al. 2010, A&A, accepted
Tutukov, A. V., & Yungelson, L. R. 1981, Nauchnye Informatsii, 49, 3
Yoon, S.-C., & Langer, N. 2004, A&A, 419, 645
Yungelson, L. R., & Tutukov, A. V. 2005, ARep, 49, 871
Webbink, R. F. 1984, ApJ, 277, 355

Appendix A: Atmospheric parameters

Table A.1. Atmospheric parameters.

Object	$T_{\rm eff}$ [K]	$\log g$	$\log y$	Instrument
J0023−0029	30100 ± 500	5.62 ± 0.08	−2.0	SDSS
	29000 ± 100	5.71 ± 0.02	−2.0	ISIS
	29200 ± 500	5.69 ± 0.05	−2.0	adopted
J1138−0035	30800 ± 500	5.50 ± 0.09	−3.0	SDSS
	31700 ± 700	5.59 ± 0.10	−3.0	IDS
	31200 ± 600	5.54 ± 0.09	−3.0	adopted
J1505+1108	33300 ± 500	5.80 ± 0.10	−2.4	SDSS
	33000 ± 600	5.80 ± 0.11	−2.2	TWIN
	33200 ± 500	5.80 ± 0.10	−2.3	adopted
J1654+3037	24400 ± 800	5.32 ± 0.11	−2.3	SDSS
	25500 ± 900	5.47 ± 0.13	−2.5	IDS
	24900 ± 800	5.39 ± 0.12	−2.4	adopted
J1726+2744	33500 ± 400	5.71 ± 0.09	−2.2	SDSS
	33300 ± 400	5.91 ± 0.06	−2.2	TWIN
	32300 ± 100	5.87 ± 0.02	−2.2	ISIS
	32400 ± 700	5.73 ± 0.12	−2.1	IDS
	32600 ± 500	5.84 ± 0.05	−2.2	adopted
J2046−0454	31600 ± 600	5.55 ± 0.10	−3.0	SDSS
	32100 ± 500	5.57 ± 0.09	−3.0	TWIN
	31100 ± 400	5.52 ± 0.06	−3.0	FORS1
	31600 ± 500	5.54 ± 0.08	−3.0	adopted
J2256+0656	28900 ± 600	5.58 ± 0.11	−3.0	SDSS
	29200 ± 900	5.74 ± 0.09	−2.2	TWIN
	28400 ± 100	5.63 ± 0.02	−2.2	ISIS
	28500 ± 500	5.64 ± 0.05	−2.3	adopted

Appendix B: Radial velocities.

Table B.1. J0023−0029.

Mid−HJD −2 450 000	RV [km s^{-1}]	Instrument
1816.782390	92.0 ± 10.0	SDSS
1816.794497	94.1 ± 6.0	
1816.806476	92.7 ± 7.0	
1885.575567	5.6 ± 9.0	
1885.587847	2.2 ± 11.0	
1885.600718	2.4 ± 15.0	
1885.614294	−3.1 ± 9.0	
1885.627153	7.7 ± 9.0	
1885.639444	−9.0 ± 8.0	
1899.578750	−36.7 ± 14.0	
1899.590972	−17.2 ± 9.0	
1899.603316	−27.7 ± 10.0	
1899.615509	−12.1 ± 11.0	
1900.573652	−13.8 ± 7.0	
1900.585712	−9.6 ± 22.0	
1900.599109	−25.3 ± 16.0	
5068.61892	90.6 ± 3.0	ISIS
5068.62614	94.8 ± 3.7	
5068.63335	81.4 ± 4.0	
5068.65013	102.0 ± 4.0	
5068.65736	103.5 ± 4.4	
5068.66457	94.9 ± 3.7	
5069.69141	−25.4 ± 4.6	
5069.69862	−65.8 ± 4.1	
5069.70585	−32.1 ± 2.9	
5069.71578	−28.2 ± 2.6	
5069.72300	−17.9 ± 4.3	
5069.73023	−6.2 ± 4.1	
5071.59347	71.9 ± 5.9	
5071.60068	79.3 ± 6.4	
5071.60442	84.1 ± 4.2	
5071.61757	91.7 ± 5.8	
5071.62478	100.7 ± 2.6	
5071.63199	93.9 ± 3.2	
5144.55811	101.0 ± 10.1	EFOSC2
5144.59234	97.1 ± 10.1	
5144.63989	76.5 ± 12.6	
5145.52594	−28.5 ± 9.9	
5145.61524	−16.9 ± 7.8	
5145.65247	−7.1 ± 10.2	
5146.54220	2.5 ± 8.0	
5146.64161	−27.0 ± 8.1	
5146.69219	−57.2 ± 8.9	
5147.59722	82.4 ± 10.4	
5147.64906	81.5 ± 9.5	
5147.66103	85.2 ± 7.2	
5147.67897	80.0 ± 9.8	

Table B.2. J1138−0035.

Mid−HJD −2 450 000	RV [km s^{-1}]	Instrument
1629.831447	−16.0 ± 33.7	SDSS
1629.861748	−131.2 ± 5.8	
1629.875990	−139.6 ± 10.5	
1629.890197	−124.6 ± 11.9	
1630.849549	42.3 ± 12.3	
1630.861782	−8.6 ± 5.8	
1658.666991	16.0 ± 6.1	
1658.723102	−127.9 ± 2.4	
1658.737309	−120.4 ± 7.4	
1658.749439	−81.3 ± 12.2	
2720.30421	−73.0 ± 32.8	SAAO
2720.31674	−9.9 ± 12.2	
3101.42483	166.9 ± 29.9	
3101.44590	26.1 ± 19.6	
4186.50643	−146.0 ± 5.5	IDS
4186.52047	−130.5 ± 6.5	
4187.51138	−76.5 ± 6.8	
4187.52540	−133.0 ± 6.8	
4188.55849	−115.9 ± 5.6	
4188.57251	−135.0 ± 6.5	
4189.46081	4.8 ± 5.2	
4189.47485	69.2 ± 5.2	
4190.52859	117.1 ± 6.0	
4190.54262	165.7 ± 5.1	
4991.40638	149.6 ± 18.6	IDS
4991.40999	143.0 ± 15.0	
4991.41360	151.1 ± 15.8	
4991.41722	148.4 ± 15.0	
4991.42083	163.3 ± 18.2	
4991.42444	162.0 ± 18.4	
4991.42964	182.6 ± 15.9	
4991.43325	172.7 ± 21.8	
4991.43687	192.4 ± 17.6	
4991.44048	193.8 ± 18.3	
4991.44409	156.9 ± 18.8	
4991.44770	169.9 ± 15.0	
4991.45131	151.1 ± 17.2	
4991.45492	151.7 ± 17.4	
5240.64268	38.5 ± 8.5	Goodman
5240.64678	59.9 ± 7.0	
5240.65068	59.2 ± 5.1	
5240.65448	108.3 ± 8.6	
5240.65828	116.8 ± 3.6	
5240.75829	−13.8 ± 5.3	
5240.76549	−49.6 ± 5.5	

Table B.3. J1505+1108.

Mid−HJD −2 450 000	RV [km s^{-1}]	Instrument
3848.858414	5.3 ± 12.0	SDSS
3848.906794	27.7 ± 12.2	
3849.863669	−126.6 ± 10.0	
3850.893113	−96.1 ± 8.1	
4600.479632	−48.0 ± 8.0	TWIN
4600.487332	−65.4 ± 10.0	
4692.348022	22.2 ± 13.0	
4694.404665	−44.7 ± 9.7	
4696.399472	−148.2 ± 10.8	
4980.44927	−130.0 ± 9.2	
4980.53561	−175.5 ± 9.9	
4981.57813	−34.5 ± 13.8	
4982.55136	5.4 ± 12.1	
4936.672663	−37.3 ± 2.8	GMOS
4936.676403	−31.0 ± 3.0	
4936.680142	−34.7 ± 3.0	
4936.683881	−32.5 ± 3.1	
4936.871029	−3.5 ± 2.8	
4936.874768	−2.1 ± 2.8	
4936.878512	0.9 ± 2.8	
4936.882253	−5.5 ± 2.9	
4937.64103	0.8 ± 3.1	
4937.64477	7.0 ± 2.9	
4937.64852	6.1 ± 3.0	
4937.65226	4.4 ± 2.9	
4937.85083	−158.7 ± 2.9	
4937.85457	−161.9 ± 2.9	
4937.85831	−158.5 ± 2.9	
4937.86206	−158.7 ± 3.0	
4938.75627	−150.6 ± 2.5	
4938.76001	−149.4 ± 2.5	
4938.76375	−156.3 ± 2.5	
4938.76749	−146.0 ± 2.5	
4939.67990	−31.1 ± 2.8	
4939.68364	−24.8 ± 2.9	
4939.68738	−26.7 ± 2.8	
4939.69112	−23.6 ± 2.8	
4943.63233	−2.9 ± 3.0	
4943.63607	−9.2 ± 2.9	
4943.63981	−7.8 ± 2.9	
4943.64355	−10.3 ± 2.7	

Table B.4. J1654+3037.

Mid−HJD −2 450 000	RV [km s^{-1}]	Instrument
2789.917095	119.4 ± 9.7	SDSS
2789.933032	84.5 ± 7.7	
2790.913235	146.7 ± 7.2	
2790.929502	130.3 ± 8.5	
4586.567656	−6.0 ± 7.8	TWIN
4692.367579	155.2 ± 8.0	
4693.380826	148.1 ± 8.1	
4694.433521	155.9 ± 8.0	
5037.44285	70.1 ± 10.6	
5037.47019	150.9 ± 8.4	
5037.50213	156.2 ± 11.1	
5038.42271	−21.8 ± 11.0	
5038.48616	155.0 ± 10.8	
5038.49857	161.0 ± 7.9	
4988.47623	−4.3 ± 25.5	IDS
4988.49036	56.8 ± 16.6	
4988.50437	97.9 ± 17.5	
4988.52125	129.9 ± 15.6	
4988.53530	172.6 ± 17.3	
4988.54942	179.7 ± 18.0	
4988.56430	150.0 ± 16.0	
4991.47179	−84.8 ± 17.7	
4991.47888	−82.0 ± 17.1	
4991.48596	−92.2 ± 16.6	
4991.49305	−58.5 ± 7.1	
4991.50013	−62.6 ± 17.5	
4991.50927	−44.1 ± 16.5	
4991.51753	−11.2 ± 15.1	
4991.52577	23.0 ± 18.4	
4991.53402	33.3 ± 16.2	
4991.54224	66.3 ± 16.0	
4991.55155	103.8 ± 30.1	
4991.55981	128.0 ± 17.6	
4991.56805	142.9 ± 16.5	
4991.57629	161.2 ± 17.1	
4991.58453	178.5 ± 16.4	

Table B.5. J1726+2744.

Mid−HJD −2 450 000	RV [km s⁻¹]	Instrument
3905.819525	−168.9 ± 10.9	SDSS
3905.833513	−157.3 ± 10.7	
3905.853553	−133.2 ± 10.5	
3905.866007	−123.5 ± 15.8	
4979.59252	−125.2 ± 14.4	TWIN
4979.63382	−98.5 ± 11.6	
4980.47951	−155.4 ± 12.9	
4980.58604	−141.2 ± 11.4	
4981.53132	−120.0 ± 8.0	
4981.58892	−112.5 ± 12.9	
4981.62939	−46.7 ± 12.0	
4981.64123	−53.1 ± 9.7	
4981.65164	−35.2 ± 16.9	
4982.56453	−154.2 ± 11.2	
4982.65151	-65.0 ± 21.6	
4983.53806	−152.7 ± 11.5	
4983.54720	−176.7 ± 12.0	
4983.55638	−150.5 ± 15.2	
4983.56557	−146.3 ± 24.3	
4983.57468	−124.9 ± 13.8	
5037.45679	39.0 ± 12.0	
5037.48545	62.0 ± 12.7	
5038.43771	38.0 ± 16.1	
5038.45381	58.0 ± 12.9	
5038.47045	80.0 ± 13.0	
5039.49762	69.0 ± 12.7	
5039.52128	87.0 ± 12.0	
5039.53838	85.0 ± 12.9	
4992.48445	−99.5 ± 23.1	IDS
4992.49617	−114.1 ± 18.5	
4992.50788	−81.2 ± 13.7	
5068.47186	−92.7 ± 5.2	ISIS
5068.47906	−79.4 ± 4.4	
5068.48628	−73.9 ± 5.3	
5069.45355	−120.3 ± 3.2	
5069.46426	−109.9 ± 2.7	
5069.46786	−98.2 ± 4.5	
5069.47855	−79.9 ± 3.8	

Table B.6. J2046-0454.

Mid−HJD −2 450 000	RV [km s⁻¹]	Instrument
3269.661429	109.6 ± 13.3	SDSS
3269.675556	128.1 ± 9.6	
3269.691435	179.6 ± 8.8	
4645.79103	181.6 ± 5.0	FORS1
4645.79259	185.0 ± 3.1	
4692.51274	28.4 ± 13.4	TWIN
4692.52696	30.7 ± 14.3	
4693.42472	227.7 ± 11.9	
4693.47199	137.2 ± 20.6	
4696.49294	42.0 ± 9.3	
4696.54469	177.8 ± 10.9	
4696.60171	171.6 ± 9.8	
4979.61251	90.6 ± 6.8	
4979.65127	−32.8 ± 21.3	
5035.46989	207.0 ± 15.3	
5035.49811	210.0 ± 14.3	
5036.50301	83.0 ± 15.5	
5037.52184	−25.0 ± 10.8	
5037.59514	16.0 ± 15.0	
4758.55029	206.1 ± 22.5	EFOSC2
4758.55416	202.4 ± 25.3	
4758.55803	212.2 ± 22.5	

Table B.7. J2256+0656.

Mid−HJD −2 450 000	RV [km s^{-1}]	Instrument
3710.557488	11.8 ± 10.5	SDSS
3710.571464	1.1 ± 8.6	
3710.588935	−15.5 ± 9.7	
4694.610760	78.0 ± 6.0	TWIN
4694.676593	79.3 ± 1.0	
4694.689883	87.1 ± 6.0	
5035.48389	−140.9 ± 23.8	
5035.50848	−96.8 ± 15.6	
5036.51782	95.0 ± 15.0	
5036.61657	29.9 ± 10.7	
5036.56824	81.7 ± 11.2	
5037.53430	−129.6 ± 17.9	
5037.54784	−120.8 ± 11.1	
5037.55965	−134.9 ± 11.0	
5037.60833	−116.5 ± 11.0	
5038.56302	96.6 ± 10.6	
5038.57506	115.1 ± 12.7	
5038.62975	104.1 ± 15.3	
5038.64304	105.0 ± 11.8	
5038.65573	104.1 ± 13.1	
5039.64785	−123.9 ± 12.5	
5048.981437	16.4 ± 4.2	GMOS
5049.002417	28.5 ± 4.3	
5049.023396	43.5 ± 4.2	
5049.044376	51.0 ± 4.3	
5077.83332	129.0 ± 5.6	
5077.85483	116.5 ± 5.3	
5068.53076	−36.5 ± 3.4	ISIS
5068.53111	−30.2 ± 3.5	
5068.53826	−26.5 ± 2.3	
5068.54815	−10.3 ± 2.7	
5068.55536	−12.8 ± 3.2	
5068.56257	−1.5 ± 2.3	
5069.53785	41.6 ± 3.7	
5069.54507	48.0 ± 3.8	
5069.55228	45.8 ± 2.3	
5069.56913	48.2 ± 3.6	
5069.57635	26.9 ± 3.8	
5069.58358	18.2 ± 3.8	
5070.62493	−48.4 ± 4.0	
5070.63214	−35.8 ± 4.0	
5070.63942	−21.1 ± 4.1	
5070.65603	−20.0 ± 2.6	
5070.66324	−1.5 ± 4.5	
5070.67045	2.6 ± 4.6	
5071.39970	8.8 ± 4.8	
5071.39997	21.3 ± 4.2	
5071.40718	33.8 ± 3.6	
5071.42392	50.5 ± 3.8	
5071.43114	50.8 ± 3.9	